Mineralization of Acid Red 1 azo dye by solar photoelectro-Fenton-like process using electrogenerated HClO and photoregenerated Fe(II)

María F. Murrieta [a], Ignasi Sirés [b], Enric Brillas [b], José L. Nava *[,a]

[a] *Departamento de Ingeniería Geomática e Hidráulica, Universidad de Guanajuato, Av. Juárez 77, Zona Centro, C.P 36000, Guanajuato, Guanajuato, Mexico*

[b] *Laboratori d'Electroquímica dels Materials i del Medi Ambient, Departament de Química Física, Facultat de Química, Universitat de Barcelona, Martí i Franquès 1-11, 08028 Barcelona, Spain*

E-mail addresses: mf.murrietachagollan@ugto.mx (M. F. Murrieta)
i.sires@ub.edu (I. Sirés)
brillas@ub.edu (E. Brillas)

*Corresponding author: jlnm@ugto.mx
Tel: + 01 (473) 10 20 100, 7320 006 ext. 2289; fax: + 2209.

Abstract

The degradation of Acid Red 1 (AR1) azo dye by solar photoelectro-Fenton-like (SPEF-like) process involving continuously electrogenerated hypochlorous acid (HClO) and photoregenerated Fe(II) to yield hydroxyl radicals, has been studied. The assays were made in a flow plant included a filter-press cell equipped with a Ti|Ir–Sn–Sb oxide anode, to oxidize Cl^- ion to HClO, and a stainless-steel cathode. The cell was coupled to a compound parabolic collector (CPC) photoreactor, in series with a reservoir containing 6 L of solution. The influence of the added Fe^{2+} concentration, current density and initial AR1 content over the performance of the SPEF-like process was systematically studied. The best treatment for 0.196 mM AR1 solutions in 35 mM NaCl and 25 mM Na_2SO_4 at pH 3.0 was achieved in the presence of 0.40 mM Fe^{2+} under a current density of 15 mA cm^{-2}, which yielded total color removal at 120 min and 74% COD decay at 480 min, with 25% of average current efficiency and 0.076 kWh $(g\ COD)^{-1}$ of energy consumption. The SPEF-like process was compared with anodic oxidation with electrogenerated active chlorine (AO-HClO), electro Fenton-like (EF-like) and photoelectro-Fenton-like (PEF-like) processes, and it was found that the oxidation power decreased in the sequence: SFEF-like > PEF-like > EF-like > AO-HClO. Ion-exclusion HPLC analysis of electrolyzed solutions revealed the formation of maleic and oxalic acid as final short-chain linear carboxylic acids.

Keywords: Active chlorine; Anodic oxidation; Azo dye; Photoelectro-Fenton process; Hydroxyl radical; Water treatment

1. Introduction

Large volumes of wastewater are daily produced worldwide as a result of a vast number of industrial activities. Among them, textile industry stands out due to the high water demand for the dying processes (Holkar et al., 2016). Discharge of sewages into water bodies causes a considerable aesthetic and chemical impact that may affect the aquatic life (Willets and Ashbolt, 2000). These effluents contain different types of chemicals like acids, salts, surfactants and organic dyes, which become hazardous even at low concentrations (Barredo-Damas et al., 2006; Nidheesh et al., 2018).

Azo dyes are ubiquitous in the textile industry. They contain one or more azo groups (-N=N-) linked to aromatic rings that contain functional groups such as -OH, -CH_3 and -SO_3- in their structure (Robinson et al., 2001; Waring and Hallas, 2013). Azo dyes are toxic, mutagenic and carcinogenic compounds that originate severe ecological problems (Allen, 1995; Medvedev et al., 1988; Nidheesh et al., 2018). Due to their resistance to biodegradation, conventional biological and physicochemical treatments have not shown good removal efficiencies for these persistent organic pollutants (POPs) (Martínez-Huitle et al., 2015; Espinoza et al., 2016; dos Santos et al., 2018). Acid Red 1 (AR1) is a commonly used azo dye (see formula and chemical characteristics in Table SM-1). It is included in the list of eleven non-biodegradable azo dyes with great resistivity towards conventional methods for wastewater treatment, which at high concentrations can be toxic and mutagenic (Daud et al., 2010, 2011; Thomas et al., 2014). Therefore, more efficient degradation methods are needed to prevent its hazardous impact on living beings.

Electrochemical advanced oxidation processes (EAOPs) have emerged as a prominent option to remove POPs, showing good performance for the mineralization of textile dyes by

the in-situ generation of strong oxidants via direct and indirect pathways (Panizza and Cerisola, 2009; Sirés et al., 2014; Brillas and Martínez-Huitle, 2015; Martínez-Huitle et al., 2015; Thiam et al., 2015; Holkar et al., 2016). The main oxidant produced in the EAOPs is the hydroxyl radical ($^{\bullet}OH$), with a high standard redox potential ($E°$= 2.87 V/SHE) and non-selectiveness, thus showing great ability to eliminate a wide variety of POPs (Panizza and Cerisola, 2009; Sirés and Brillas, 2012; Sirés et al., 2014; Brillas and Martínez-Huitle, 2015).

Among the EAOPs, the Fenton-based treatments have recently received great attention. Such processes are based on the $^{\bullet}OH$ production via Fenton's reaction between Fe^{2+} and electrogenerated hydrogen peroxide (H_2O_2) in acidic media (Galia et al., 2016; Lanzalaco et al., 2017). The most common Fenton-based EAOPs are electro-Fenton (EF), photoelectro-Fenton (PEF) and solar photoelectro-Fenton (SPEF), which have shown high effectiveness for the remediation of wastewater containing POPs (Sirés and Brillas, 2012, 2017; Brillas, 2014; Pérez et al., 2017; Coria et al., 2018).

The presence of chloride ion in textile wastewater allows the production of active chlorine, namely HClO and/or ClO^-, during the Fenton-based treatments, thereby competing with the $^{\bullet}OH$ to attack the pollutants. Active chlorine is formed by anodic oxidation of Cl^- ion via reactions (1)-(3). The predominant species depends on the solution pH, which eventually determines the oxidation power of the treatment. The most powerful species is HClO ($E°$ = 1.49 V/SHE), prevalent at pH between 3 and 8, followed by Cl_2(aq) ($E°$=1.36 V/SHE). In contrast, the weakest species is ClO^- ($E°$ = 0.89 V/SHE), which prevails beyond pH 8 (Trasatti, 1987).

$$2Cl^- \rightarrow Cl_2(aq) + 2e^- \quad (1)$$

$$Cl_2(aq) + H_2O \rightarrow HClO + Cl^- + H^+ \quad (2)$$

81 $HClO \leftrightarrows ClO^- + H^+ \qquad pK_a = 7.45 \qquad (3)$

82 Kishimoto and Sugimura (2010) reported the Fenton-like reaction between HClO and
83 Fe^{2+} to produce $^{\bullet}OH$ in the bulk solution according to reaction (4), where the classical
84 Fenton's reaction is mimicked upon replacement of H_2O_2 by HClO. It is important to
85 highlight that only a limited number papers have focused on this Fenton-like process for the
86 destruction of POPs (Candeias et al., 2009; Kishimoto and Sugimura, 2010, 2013; Coledan
87 2018). In earlier work, Aguilar et al. (2017) reported an electrochemical approach to this
88 process, producing anodically the HClO through the oxidation of Cl^- on a Ti|Ir–Sn–Sb oxide
89 electrode via reactions (1) and (2). There was evidence of the EF-like process during the
90 oxidation of the Acid Yellow 36 azo dye, attaining good results in terms of color removal
91 and TOC decay.

92 $HClO + Fe^{2+} \rightarrow Fe^{3+} + {}^{\bullet}OH + Cl^- \qquad (4)$

93 As in classical EF, the Fenton-like reaction (4) can be propagated from Fe^{2+} regeneration
94 by cathodic reduction via reaction (5) (Panizza and Oturan, 2011):

95 $Fe^{3+} + e^- \rightarrow Fe^{2+} \qquad (5)$

96 This EF-like process avoids the use of a gas diffusion cathode, commonly employed to
97 electrogenerate hydrogen peroxide, and a more simple and cheaper platinized Ti or a
98 stainless-steel plate can be utilized instead. Furthermore, by-products such as $Fe(OH)^{2+}$ and
99 Fe(III)-carboxylate are produced in such EF-like treatment, decreasing its effectiveness.
100 These Fe(III) by-products can be photoreduced to Fe(II) upon irradiation with a source of
101 UVA light through reactions (6) and (7) in the so-called PEF-like process, enhancing the
102 mineralization of organic pollutants (Sirés et al., 2014; Aguilar et al., 2017; Xu et al., 2019).

$$Fe(OH)^{2+} + h\nu \rightarrow Fe^{2+} + {}^{\bullet}OH \quad (6)$$

$$Fe(OOCR)^{2+} + h\nu \rightarrow Fe^{2+} + CO_2 + R^{\bullet} \quad (7)$$

A disadvantage of PEF is that the use of UVA lamps entails an additional electric energy consumption. This is overcome in the SPEF process, since sunlight is utilized as an inexpensive and renewable energy source. The SPEF treatment of POPs with electrogenerated H_2O_2 and Fe^{2+} has been widely studied, showing excellent performance (Thiam et al., 2015; Pérez et al., 2017). However, the performance of a SPEF-like process involving electrogenerated HClO and photoregenerated Fe(II) has not been evaluated yet. Hence, EF-like, PEF-like and SPEF-like processes seem good alternative methods to conventional EF, PEF and SPEF when the solutions contain chloride, as is the case of industrial textile wastewater.

This work reports the degradation of AR1 azo dye by SPEF-like process with anodically produced HClO and photoregenerated Fe(II) at pH 3.0 to yield $^{\bullet}OH$. The trials were carried out in a 6 L pre-pilot plant composed of an FM01-LC filter-press flow cell, with a Ti|Ir–Sn–Sb oxide anode and a stainless-steel cathode, connected to a compound parabolic collector (CPC) photoreactor, operating in recirculation batch mode. The influence of catalyst (Fe^{2+}) concentration, current density (j) and initial AR1 concentration on the performance of the SPEF-like process was assessed. Comparative trials by anodic oxidation with electrogenerated HClO (AO-HClO), EF-like and PEF-like processes were made to clarify the role of reaction (4) in the presence of Fe^{2+}. Generated carboxylic acids were identified by ion-exclusion high-performance liquid chromatography (HPLC). The effect of j on the accumulation of HClO from Cl^- oxidation at the Ti|Ir–Sn–Sb oxide anode was also assessed.

2. Materials and methods

2.1. Chemicals

Commercial Acid Red 1 was supplied by Sigma-Aldrich and used as received. The electrolytic solutions were prepared with deionized water. Na_2SO_4 and NaCl were purchased from Karal and used as supporting electrolytes, $FeSO_4 \cdot 7H_2O$ was supplied by Fermont and used as catalyst. Chemicals used for analysis were of analytical grade purchased from Sigma-Aldrich.

2.2. Electrochemical system

The pre-pilot plant used in this work, designed and constructed by ourselves, has been described elsewhere (Pérez et al., 2017). It was composed of an FM01-LC electrochemical flow reactor coupled to a CPC photoreactor and a stirred tank that contained 6 L of solution, which was recirculated through the system by a centrifugal pump. The solution first reached the electrochemical reactor, then the photoreactor and finally, it was sent to the reservoir. The FM01-LC reactor was equipped with a Ti|Ir–Sn–Sb oxide plate as the anode, prepared as reported in earlier work (Aguilar et al., 2018), and a stainless-steel plate as the cathode. Both electrodes had a geometric area of 64 cm^2 and the interelectrode gap was of 0.55 cm, where a Type-D turbulence promoter was positioned (Rivera et al., 2015). All trials were carried out at constant *j* provided by a BK Precision 1621A DC power supply, which displayed the voltage between the electrodes.

Duplicated trials were comparatively performed by AO-HClO, EF-like, PEF-like and SPEF-like using solutions containing AR1 in 35 mM NaCl + 25 mM Na_2SO_4 as background electrolyte at initial pH of 3.0. This pH value was selected because it has been found as the optimal for Fenton-based processes (Sirés et al., 2014). The AO-HClO and EF-like runs were

made in the dark, covering the system with an opaque cloth. The PEF-like experiments were conducted using a 15-W black light UVA lamp with λ_{max} = 365 nm, which irradiated the CPC photoreactor locked in a black box. The SPEF-like assays were performed in clear and sunny days during the spring of 2019. The average daily UV solar irradiance was measured at a weather station located at the University of Guanajuato and was around 55 W m^{-2}. The effect of Fe^{2+} concentration, applied *j* and AR1 content on the performance of the latter treatment was assessed.

2.3. Apparatus and analytical methods

The solution pH was adjusted to 3.0 with a 10% (v/v) H_2SO_4 solution, as determined using a Hanna HI991300 pH-meter. Samples were withdrawn at different time intervals and further degradation inside the vials was immediately prevented by adding a 10% (v/v) NaOH solution until alkaline pH values were reached. The resulting solutions were filtered with 0.45 μm PTFE syringe filters before analysis. The decolorization of AR1 solutions was monitored from the absorbance decay (at λ_{max} = 506 nm, according to the absorption spectrum of the dye) measured on a Perkin Elmer Lambda 35 UV/Vis spectrophotometer. The percentage of color removal was then calculated from Eq. (8):

$$\%\ \text{Color removal} = \frac{A_0 - A_t}{A_0} 100 \quad (8)$$

where A_0 is the initial absorbance and A_t is that at electrolysis time *t*. The solution COD was measured by the closed reflux dichromate titration method (APWA, AWWA, WEF, 1992).

Produced carboxylic acids were detected and quantified by ion-exclusion HPLC using a Perkin Elmer Flexar LC fitted with an Agilent Hi-Plex H 8 mm, 300mm × 7.7 mm (i.d.), column at room temperature and coupled with a Flexar photodiode array detector set at λ =

210 nm. These analyses were carried out by injecting 20 μL of sample into the LC, being eluted with a 4 mM H_2SO_4 solution as mobile phase at 0.6 mL min^{-1} (Pérez et al., 2017).

Active chlorine was measured by the standard *N*,*N*-diethyl-*p*-phenylenediamine (DPD) colorimetric method using the above UV/Vis spectrophotometer set at λ = 515 nm (APWA, 2005).

3. Results and discussion

3.1. Influence of current density on the accumulation of active chlorine

A first series of trials was carried out to assess the ability of the electrochemical system the produce active chlorine (HClO at pH 3.0) through Cl^- oxidation by reactions (1) and (2). The experiments were made with the FM01-LC reactor coupled to a stirred tank containing 6 L of a 35 mM NaCl + 25 mM Na_2SO_4 solution at pH 3.0. A high flow rate of 3.2 L min^{-1} was used to avoid stagnant zones inside the FM01-LC reactor (Rivera et al., 2015). Fig. SM-1 shows the influence of *j* from 5 to 20 mA cm^{-2} on the accumulation of active chlorine. It can be observed that the concentration of accumulated HClO increased with raising *j*, attaining 0.44, 0.64, 1.90 and 2.22 mM after 360 min of electrolysis at 5, 10, 15 and 20 mA cm^{-2}, respectively. However, low current efficiencies of 8%, 7%, 12% and 11% were obtained, which can be related to the simultaneous O_2 evolution, the $^{\bullet}OH$-mediated or direct oxidation of HClO to produce ClO_3^- and ClO_4^- ions (Thiam et al., 2015; Steter et al., 2016; Aguilar et al., 2017), the partial Cl_2 stripping from the solution, and the cathodic reduction of active chlorine (Vacca et al., 2013).

The electrogenerated active chlorine in the pre-plant with the Ti|Ir–Sn–Sb oxide anode in the presence of Cl^- ion at pH 3.0 is then expected to be a relevant oxidant to promote the

degradation of AR1 azo dye and its intermediates by AO-HClO, EF-like, PEF-like and SPEF-like processes (Aguilar et al., 2017), as discussed in the next subsections.

3.2. Effect of Fe^{2+} concentration on the SPEF-like process

To ascertain the influence of catalyst concentration on the SPEF-like process, 6 L of 0.196 mM AR1 (4.06 mM COD) solutions with 35 mM NaCl + 25 mM Na_2SO_4 and 0.1-0.50 mM Fe^{2+} were electrolyzed in the plant at j = 15 mA cm^{-2} and volumetric flow rate of 3.2 L min^{-1} for 480 min. The electrolyses were run at that current density because of the good accumulation up to 1.90 mM HClO, which ensures the continuous occurrence of the Fenton-like reaction (4). The fixed flow rate prevented the appearance of stagnant zones, both in the FM01-LC electrochemical reactor (Rivera et al., 2015) and the CPC (Pérez and Nava, 2018), aiming at an excellent performance of the system (Pérez et al., 2017; Coria et al., 2018).

Fig. 1a shows the percentage of color decay versus electrolysis time for the above assays. As can be seen, the presence of a higher Fe^{2+} concentration caused a gradual deceleration of the decolorization process, more significantly at contents ≥ 0.30 mM. The quicker loss of color in the absence of catalyst suggests that active chlorine produced via reactions (1) and (2) was the main oxidant to break the azo bond, whereas the heterogeneous hydroxyl radical M(•OH) generated via reaction (9) also occurring at the Ti|Ir–Sn–Sb oxide anode surface (Aguilar et al., 2018, 2019) had a smaller relevance. Upon Fe^{2+} addition, HClO was partly consumed from reaction (4) and hence, a lower content of this oxidant was available to attack the azo dye and its oxidation products, yielding a slower decolorization.

$$M + H_2O \rightarrow M(^{\bullet}OH) + H^+ + e^- \quad (9)$$

Fig. 1b depicts the normalized COD decay with time at the different Fe^{2+} concentrations studied. As can be seen, COD removal was upgraded with increasing catalyst content and thus, at 0.10, 0.20, 0.30 and 0.40 mM Fe^{2+} it was finally abated by 59%, 61%, 68% and 74%, respectively. These values were much higher than 29% obtained in the absence of Fe^{2+} ion (i.e., under AO-HClO conditions). This is a clear evidence of the progressive improvement of •OH production in the bulk from reactions (4)-(6), which can yield a larger oxidation of the organics. Nevertheless, when the catalyst concentration was further increased up to 0.50 mM Fe^{2+}, COD abatement became poorer, only being reduced by 50%. This suggests that the excess of Fe^{2+} promoted a large acceleration of the parasitic reaction (10) causing its consumption by •OH, leading to a decrease of the process efficiency (Sirés and Brillas, 2012, 2017; Sirés et al., 2014).

$$Fe^{2+} + {}^{\bullet}OH \rightarrow Fe^{3+} + OH^{-} \quad (10)$$

From the above COD measurements, two important parameters like the average current efficiency (ACE) and the energy consumption (EC) were calculated (Brillas et al., 2017). The ACE (in percentage) was determined according to Eq. (11):

$$\%\,\mathrm{ACE} = \frac{(\Delta \mathrm{COD})_t F V_s}{8It} 100 \quad (11)$$

where F is the Faraday constant (96,485 C mol^{-1}), V_s is the solution volume (L), $(\triangle \mathrm{COD})_t$ is the experimental COD decay (g O_2 L^{-1}), 8 is the oxygen equivalent mass (g eq^{-1}), I is the current intensity (A) and t is electrolysis time (s) at which sample was taken. The EC value was calculated from Eq. (12):

$$\mathrm{EC}\ (\mathrm{kWh}\ (\mathrm{g\ COD})^{-1} = \frac{E_{cell} I t}{(\triangle \mathrm{COD})_t V_s} \quad (12)$$

where E_{cell} accounts for the average cell potential (V).

Fig. 1c shows the evolution of ACE with time for the above trials. The highest ACE was obtained at 0.40 mM Fe^{2+}, with a value as high as 123% at the beginning of the SPEF-like process, thereby dropping down to 25% at 480 min. That catalyst amount can then be considered as the optimal to ensure the best treatment of AR1 solutions. Lower, but gradually increasing ACE values up to 58%, 72% and 82% were attained when employing 0.10, 0.20 and 0.30 mM Fe^{2+}, respectively. It is important to notice that the use of 0.50 mM Fe^{2+} caused a strong decay of the initial ACE, whose value was 41%, still superior to 30% determined in AO-HClO (without catalyst). This behaviour confirms the increasing formation of $^{\bullet}OH$ from Fenton-like reaction (4), sustained by reactions (5) and (6), thus upgrading the ACE values up to 0.40 mM Fe^{2+}; in contrast, the detrimental effect of reaction (10) affected the efficiency in the trial with 0.50 mM Fe^{2+}. At the beginning of the treatment at 0.40 mM Fe^{2+}, the ACE values greater than 100% found can be explained by: (i) The combined effect of reactions (1), (2) and (4), along with (ii) the crucial contribution of photochemical reactions (6) and (7) promoted by UVA light, which allow the destruction of refractory complexes and the continuous photoregeneration of Fe^{2+} catalyst, and (iii) the low current density employed (j = 15 mA cm^{-2}). The fast decay of ACE as the electrolysis was prolonged, as observed in all the trials of Fig. 1c, can be justified by the loss of organic load with generation of more refractory by-products (Sirés et al., 2014; Coria et al., 2018).

Fig. 1d highlights, as expected, that EC rose at longer electrolysis time and it became lower as greater COD abatements were achieved. The lowest final EC was found for the optimum trial at 0.40 mM Fe^{2+}, only requiring 0.076 kWh $(g\ COD)^{-1}$ to achieve 74% COD decay. In the absence of Fe^{2+} (i.e., AO-HClO process), the final EC was as high as 0.198

kWh (g COD)$^{-1}$, related to 28% COD removal, which corroborated the greater oxidation ability of the SFEF-like process. It is important to highlight that the direct photolysis of the AR1 azo dye under solar irradiation was completely ineffective, in agreement with other studies that reported the high stability of this class of dye against solar irradiation and other conventional physicochemical methods (Daud et al., 2010, 2011; Thomas et al., 2014).

3.3. Influence of current density on the SPEF-like process

Current density is a key operational variable because it determines the production of active chlorine from reactions (1) and (2). To clarify its effect on the degradation of AR1 by SPEF-like process, several trials were carried out by electrolyzing a 0.196 mM dye solution with 35 mM NaCl + 25 mM Na_2SO_4 and 0.40 mM Fe^{2+} as optimum catalyst concentration, at *j* values of 5, 10, 15 and 20 mA cm^{-2}.

Fig. 2a clearly evidences an enhancement of the percentage of color removal as *j* became higher. This can be explained by the greater amount of active chlorine produced, as shown in Fig. SM-1, simultaneously increasing the •OH content via Fenton-like reaction (4). At 5 and 10 mA cm^{-2}, 89% and 98% of decolorization percentages were attained after 240 min of electrolysis, respectively, whereas at higher *j* values of 15 and 20 mA cm^{-2}, more than 97% color removal was already achieved at 120 min.

Fig. 2b shows the expected rise of the normalized COD decay with increasing *j*, reaching final values of 50%, 56% and 74% at 5, 10 and 15 mA cm^{-2}. However, a lower COD abatement was obtained at 20 mA cm^{-2} (61%) as compared to the latter trial, which can be associated with the quicker increase in rate of (i) the O_2 evolution reaction, (ii) the •OH-mediated and direct oxidation of active chlorine, and/or (iii) the parasitic reaction (10).

Fig. 2c highlights that similar initial ACE values around 120% were determined at the beginning of the processes at j between 5 and 15 mA cm^{-2}, which decayed to 80% at 20 mA cm^{-2} because of the higher acceleration of side reactions, as stated above. The ACE value always decayed monotonically at longer time, more rapidly with increasing j, which can be associated with the quicker formation of more recalcitrant by-products upon the action of greater amounts of generated oxidants (mainly HClO and $^{\bullet}OH$). This behavior is also evident from the profiles of EC presented in Fig. 2d, whose values progressively rose with increasing j due to the associated greater E_{cell} (see Eq. (12)), varying between 0.023 and 0.140 kWh (g $COD)^{-1}$ within the j range from 5 to 20 mA cm^{-2}.

The above findings allow concluding that under the present experimental conditions using an optimum Fe^{2+} catalyst concentration (0.40 mM), the SPEF-like process performed better at j = 15 mA cm^{-2}, since it yielded the largest COD abatement of 74% with a relatively low EC of 0.076 kWh (g $COD)^{-1}$. These were considered the best conditions, being kept in subsequent assays.

3.4. Effect of Acid Red 1 concentration on the SPEF-like process

The influence of the AR1 concentration between 0.096 mM (2.03 mM COD) and 0.385 mM (8.12 mM COD) on the performance of the SPEF-like treatment was assessed. Fig. 3a shows that using 0.40 mM Fe^{2+} as catalyst and operating at j = 15 mA cm^{-2}, total decolorization of 0.096 and 0.196 mM dye solutions was reached in 120 min of electrolysis, whereas the solution with 0.385 mM AR1 needed much longer time, around 480 min. This is not surprising because a constant amount of oxidizing agents is expected to be produced under the same electrolytic conditions and then, the oxidation of AR1 and its by-products became slower at greater organic load. This trend can also be observed in Fig. 3b for the

corresponding COD removals, where increasing reductions of 41%, 74% and 87% were obtained at the end of the assays of 0.385, 0.196 and 0.096 mM AR1, respectively. This behavior is opposite to the change of ACE shown in Fig. 3c, which decreased progressively as dropping the dye content. Note that an initial ACE value as high as 196% was found at 0.385 mM, decaying down to 66% at 0.096 mM. That means that a higher organic load promotes a larger interaction between the organic molecules and the oxidants (HClO and $^{\bullet}$OH), which increases the efficiency although at the expense of a longer time needed for a given COD removal (Sirés et al., 2014). This tendency fully agreed with the lower EC value obtained as the AR1 concentration became higher, as shown in Fig. 3d.

3.5. Comparative degradation of Acid Red 1 by EF-like and PEF-like treatments

Once studied the performance of the SPEF-like treatment of AR1 solutions in chloride medium at pH 3.0, comparative EF-like and PEF-like treatments of 6 L of solutions containing 0.196 mM of dye with 35 mM NaCl + 25 mM Na_2SO_4 and 0.40 mM Fe^{2+} were also carried out at j = 15 mA cm^{-2}.

Fig. 4a depicts the change of color removals in these trials, as well as those obtained in the analogous AO-HClO and SPEF-like treatments already presented in Fig. 1a. As can be seen, a slightly quicker color removal occurred in EF-like as compared to AO-HClO, both processes yielding a slightly faster decolorization than PEF-like process. A substantially slower color removal can be observed in SPEF-like treatment. This behavior suggests a pre-eminent control of color removal in AO-HClO by active chlorine production, with a smaller contribution of M($^{\bullet}$OH) formed from reaction (7). In EF-like process, the amount of homogeneous $^{\bullet}$OH formed from Fenton-like reaction (4) slightly accelerated the dye removal. However, when larger $^{\bullet}$OH contents were generated induced by photoreaction (6)

upon irradiation with UVA light, the faster consumption of active chlorine by this radical caused a loss of performance in PEF-like process. This was even more evident in SPEF-like process, since the greater UV intensity of sunlight enhanced the rate of reaction (6).

Fig. 4b illustrates that for times longer than 240 min, COD depletion decreased in the sequence: AO-HClO < EF-like < PEF-like < SPEF-like, attaining 29%, 52%, 70% and 74% abatement, respectively, at the end of such processes. This trend suggests that: (i) the homogeneous $^{\bullet}OH$ in EF-like process is more effective than active chlorine to oxidize the by-products formed, most of them probably being chloroderivatives coming from the concomitant attack of active chlorine. Such intermediates are difficulty destroyed in AO-HClO, yielding the poorest COD removal; (ii) the UVA light provided by the lamp or sunlight in the photoassisted Fenton-based EAOPs not only photoregenerates Fe^{2+} with $^{\bullet}OH$ production from reaction (6), but can also photolyze photoactive intermediates like Fe(III) complexes, reaction (7), enhancing the COD decay (Brillas et al., 2009; Sirés et al., 2014; Aguilar et al., 2017); and (iii) the greater UV intensity of sunlight can explain the slightly superior performance of SPEF-like process over PEF-like one at times greater than 240 min. The larger COD decay found in the latter process at shorter times could be due to the faster photolysis of some by-products absorbing at a wavelength near 360 nm, as supplied by the UVA lamp.

Fig. 4c confirms that the highest ACE values were achieved at the beginning of the PEF-like and SPEF-like treatments, reaching values of 199% and 123%, respectively. These high ACE can be ascribed to the combined action of electrogenerated HClO and the photoregenerated Fe(II) via reaction (6). In contrast, at the end of these trials, ACE was reduced down to 24% and 25%, being slightly greater for SPEF-like. A much better

performance of both photoassisted processes due to the photolysis of intermediates as compared to EF-like one can also be observed in Fig. 4c. For the latter process, a much slower ACE decay, from 36% to 18%, occurred, indicating a smaller influence of the destruction of the recalcitrant intermediates on its performance. In the case of the less powerful AO-HClO, a more pronounced ACE decay, from 30% to 9.6%, took place because intermediates were more slowly removed only from the attack of M(•OH), without the additional attack of homogeneous •OH formed from Fenton-like reaction (4) in EF-like treatment. According to this behaviour, the lowest final EC values were 0.080 and 0.076 kWh (g COD)$^{-1}$ for PEF-like and SPEF-like assays, respectively. The use of the latter process is then advisable for treating wastewater containing Cl^-, since the energy consumption of the former one grew up to 0.300 kWh (g COD)$^{-1}$ if the electrical power of the UVA lamp was also considered.

3.5. Identification of generated carboxylic acids

The generated carboxylic acids during the AR1 degradation were identified by ion-exclusion HPLC analysis of the solutions treated as described in Fig. 4. Any acid was detected in the photoassisted processes, whereas final oxalic and maleic acids were found in AO-HClO and EF-like treatments. Maleic acid is expected to be formed from the oxidation and cleavage of the aromatic rings of the azo dye, whereas oxalic acid is a final by-product that is produced upon degradation of long-chain aliphatic carboxylic acids (Sirés et al., 2014; Brillas and Martínez-Huitle, 2015). In the presence of iron ions, these acids are mainly in the form Fe(III)-carboxylate complexes.

Fig. 5 shows a low accumulation of maleic acid, attaining 0.37 and 0.13 mg L^{-1} at the end of the AO-HClO and EF-like treatments, respectively. Higher concentrations of oxalic acid, i.e., 1.73 and 1.55 mg L^{-1}, were finally obtained. Note that both acids were more largely

accumulated in AO-HClO, confirming the action of •OH generated from Fenton-like reaction (4) to remove their precursors in the EF-like trial. The fact that these acids were not detected in PEF-like and SPEF-like treatments can be related to the rapid photodecarboxylation of their Fe(III) complexes under UVA irradiation via reaction (7), which additionally photoregenerated Fe^{2+} that stimulated the •OH production.

4. Conclusions

The SPEF-like treatment performed in 25 mM Na_2SO_4 and 35 mM NaCl at pH 3.0 was able to completely decolorize AR1 dye solutions and largely remove their COD. A catalyst concentration of 0.40 mM Fe^{2+} and a current density of 15 mA cm^{-2} were found as optimal. The increase of dye content decelerated the decolorization process and COD removal, but enhanced the ACE and hence, decreased the EC. For 0.196 mM AR1 solutions, SPEF-like outperformed the other treatments, yielding the total decolorization at 120 min and 74% COD decay at 480 min, with 25% of ACE and EC of 0.076 kWh $(g\ COD)^{-1}$. The ACE values at short time was greater than 100%, as also found in PEF-like, suggesting the synergistic action of electrogenerated HClO and UVA photolysis. The oxidation power of EAOPs decreased in the sequence: SPEF-like > PEF-like > EF-like > AO-HClO. The superiority of EF-like as compared to AO-HClO can be related to the generation of homogeneous •OH from Fenton-like reaction (4). The photoregeneration of Fe(II) from Fe(III) species, along with the photolysis of intermediates, explains the superiority of the photoassisted treatments. The lower energy consumption of SPEF-like process makes it an interesting option for the treatment of chlorinated wastewater.

Acknowledgements

The authors gratefully acknowledge financial support from project CTQ2016-78616-R (AEI/FEDER, EU), as well as from Universidad de Guanajuato (Mexico) under the project No. 102/2019. M.F. Murrieta thanks CONACYT (Mexico) for the scholarship No. 786726 granted.

References

Aguilar, Z.G., Brillas, E., Salazar, M., Nava, J.L., Sirés, I., 2017. Evidence of Fenton-like reaction with active chlorine during the electrocatalytic oxidation of Acid Yellow 36 azo dye with Ir-Sn-Sb oxide anode in the presence of iron ion. Appl. Catal. B: Environ. 206, 44-52.

Aguilar, Z.G., Coreño, O., Salazar, M., Sirés, I., Brillas, E., Nava, J.L., 2018. Ti|Ir-Sn-Sb oxide anodes: service life and role of the acid sites content during water oxidation to hydroxyl radicals. J. Electroanal. Chem. 820, 82-88.

Allen, S.J., Khader, K.Y.H., Bino, M., 1995. Electrooxidation of dye stuffs in waste waters. J. Chem. Technol. Biotechnol. 62, 111-117.

APWA, AWWA, WEF, 1992. Standard Methods for the Examination of Water and Wastewater, 17th Ed. Method number 5220 - Chemical oxygen requirement - Closed reflux, titrimetric method, Díaz Santos S.A., Madrid, Spain. pp. 5-17 to 5-19.

APWA, AWWA, WEF, 2005. Standard Methods for the Examination of Water and Wastewater, 21st Ed. Method number 4500-Cl Chlorine (residual) – G. DPD colorimetric method, American Public Health Association, Washington D.C, USA, pp. 4–67 to 4-68.

414 Barredo-Damas, S., Alcaina-Miranda, M.I., Iborra-Clar, M.I., Bes-Pia, A., Mendoza- Roca,
415 J.A., Iborra-Clar, A., 2006. Study of the UF process as pretreatment of NF membranes
416 for textile wastewater reuse. Desalination 200, 745-747.
417 Brillas, E., 2014. A review on the degradation of organic pollutants in waters by UV
418 photoelectro-Fenton and solar photoelectro-Fenton. J. Braz. Chem. Soc. 25, 393–417.
419 Brillas, E., Sirés, I., Oturan, M., 2009. Electro-Fenton process and related electrochemical
420 technologies based on Fenton´s reaction chemistry. Chem. Rev. 109, 6570-6631.
421 Brillas, E., Martínez-Huitle, C.A., 2015. Decontamination of wastewaters containing
422 synthetic organic dyes by electrochemical methods. An updated review, Appl. Catal. B:
423 Environ. 166-167, 603-643.
424 Candeias, L.P., Stratford, M.R.L., Wardman, P., 1994. Formation of hydroxyl radicals on
425 reaction of hypochlorous acid with ferrocianide, a model iron (II) complex. Free Radic.
426 Res. 20, 241-249.
427 Coledan, D.A.C., Sánchez-Montes, I., Silva, B.F., Aquino, J.M., 2018. On the performance
428 of HOCl/Fe^{2+}, HOCl/Fe^{2+}/UVA, and HOCl/UVC processes using in situ
429 electrogenerated active chlorine to mineralize the herbicide picloram. Appl. Catal. B:
430 Environ. 227, 170-177.
431 Coria, G., Pérez, T., Sirés, I., Brillas, E., Nava, J.L., 2018. Abatement of the antibiotic
432 levofloxacin in a solar photoelectro-Fenton flow plant: modelling the dissolved organic
433 carbon concentration-time relationship. Chemosphere 198, 174-181.
434 Daud, N.K., Hameed, B.H., 2010. Decolorization of Acid Red 1 by Fenton-like process using
435 rice husk ash-based catalyst. J. Hazard. Mater. 176, 938-944.
436 Daud, N.K., Hameed, B.H., 2011. Acid Red 1 dye decolorization by heterogeneous Fenton-
437 like reaction using Fe/kaolin catalyst. Desalination 269, 291-293.

438 dos Santos, A.J., Martínez-Huitle, C.A., Sirés, I., Brillas, E., 2018. Use of Pt and boron-doped
439 diamond anodes in the electrochemical advanced oxidation of Ponceau SS diazo dye in
440 acidic sulfate medium. ChemElectroChem 5, 685-693.
441 Espinoza, C., Romero, J., Villegas, L., Cornejo-Ponce, L., 2016. Mineralization of the textile
442 dye Acid Yellow 42 by solar photoelectro-Fenton in a lab-pilot plant. J. Hazard. Mater.
443 319, 24-33.
444 Galia, A., Lanzalaco, S., Sabatino, M.A., Dispenza, C., Scialdone, O., Sirés, I., 2016.
445 Crosslinking of poly(vinylpyrrolidone) activated by electrogenerated hydroxyl radicals:
446 a first step towards a simple and cheap synthetic route of nanogel vectors. Electrochem.
447 Commun. 62, 64-68.
448 Holkar, C.R., Jadhav, A.J., Pinjari, D.V., Mahamuni, N.M., Pandit, A.B., 2016. A critical
449 review on textile wastewater treatments: possible approaches. J. Environ. Manage. 182,
450 351-366.
451 Kishimoto, N., Sugimura, E., 2010. Feasibility of an electrochemically assisted Fenton
452 method using Fe^{2+}/HOCl system as an advanced oxidation process. Water Sci. Technol.
453 62, 2321-2329.
454 Kishimoto, N., Kitamura, T., Kato, M., Otsu, H., 2013. Influence of chelating agents on
455 Fenton-type reaction using ferrous ion and hypochlorous acid. J. Water Environ.
456 Technol. 11, 21-32.
457 Lanzalaco, S., Sirés, I., Sabatino, M.A., Dispenza, C., Scialdone, O., Galia, A., 2017.
458 Synthesis of polymer nanogels by electro-Fenton process: investigation of the effect of
459 main operation parameters. Electrochim. Acta 246, 812-822.

460 Martínez-Huitle, C.A., Rodrigo, M.A., Sirés, I., Scialdone, O., 2015. Single and coupled
461 electrochemical processes and reactors for the abatement of organic water pollutants: a
462 critical review. Chem. Rev. 115, 13362-13407.
463 Medvedev, Z.A., Crowne, H.M., Medvedev, M.N., 1988. Age related variations of
464 hepatocarcinogenic effect of azo dye (3′-MDAB) as linked to the level of hepatocyte
465 polyploidization. Mech. Ageing Develop. 46, 159-174.
466 Nidheesh, P.V., Zhou, M., Oturan, M.A., 2018. An overview on the removal of synthetic
467 dyes from water electrochemical advanced oxidation processes. Chemosphere 197, 210-
468 227.
469 Panizza, M., Cerisola, G., 2009. Direct and mediated anodic oxidation of organic pollutants.
470 Chem. Rev. 109, 6541-6569.
471 Panizza, M., Oturan, M.A., 2011. Degradation of Alizarin Red by electro-Fenton process
472 using a graphite-felt cathode. Electrochim. Acta. 56, 7084-7087.
473 Pérez, T, Nava, J.L., 2018. Simulations of a single-phase flow in a compound parabolic
474 concentrator reactor. Int. J. Photoener. 2018, 2569251.
475 Pérez, T., Sirés, I., Brillas, E., Nava, J.L, 2017. Solar photoelectro-Fenton flow plant
476 modeling for the degradation of the antibiotic erythromycin in sulfate medium.
477 Electrochim. Acta 228, 45-56.
478 Rivera, F., Ponce de León, C., Nava, J.L, Walsh, F.C., 2015. The reaction environment in a
479 filter-press laboratory reactor: the FM01-LC flow cell. Electrochim. Acta 161, 436-452.
480 Robinson, T., McMullan, G., Marchant, R., Nigam, P., 2001. Remediation of dyes in textile
481 effluent: a critical review on current treatment technologies with a proposed alternative.
482 Bioresour. Technol. 77, 247-255.

Sirés, I., Brillas, E., 2012. Remediation of water pollution caused by pharmaceutical residues based on electrochemical separation and degradation technologies: a review. Environ. Int. 40, 212–229.

Sirés, I., Brillas, E., 2017. Electro-Fenton Process: Fundamentals and Reactivity, in: Zhou, M., Oturan, M.A, Sirés, I. (Eds.), Electro-Fenton process: New trends and Scale-up, Springer, Singapore, pp. 1-28.

Sirés, I., Brillas, E., Oturan, M.A., Rodrigo, M.A., Panizza, M., 2014. Electrochemical advanced oxidation processes: today and tomorrow. A review. Environ. Sci. Pollut. Res. 21, 8336-8367.

Steter, J., Brillas, E., Sirés, I., 2016. On the selection of the anode material for the electrochemical removal of methylparaben from different aqueous media. Electrochim. Acta 222, 1464-1474.

Thiam, A., Sirés, I., Centellas, F., Cabot, P.L., Brillas, E., 2015. Decolorization and mineralization of Allura Red AC azo dye by solar photoelectro-Fenton: Identification of intermediates. Chemosphere 136, 1-8.

Thiam, A., Sirés, I., Garrido, J.A., Rodríguez, R.M., Brillas, E., 2015. Effect of anions on electrochemical degradation of azo dye Carmoisine (Acid Red 14) using a BDD anode and air-diffusion cathode. Sep. Purif. Technol. 140, 43-52.

Thomas, S., Sreekanth, R., Sijumon, V.A., Aravind, U.K., Aravindakumar, C.T., 2014. Oxidative degradation of Acid Red 1 in aqueous medium. Chem. Eng. J. 244, 473-482.

Trasatti, S., 1987. Progress in the understanding of the mechanism of chlorine evolution at oxide electrodes. Electrochim. Acta. 32, 369-382.

505 Vacca, A., Mascia, M., Palmas, S., Mais, L., Rizzardini, S., 2013. On the formation of
506 bromate and chlorate ions during electrolysis with boron doped diamond anode for
507 seawater treatment. J. Chem. Technol. Biotechnol. 88, 2244-2251.
508 Waring, D.R., Hallas, G., 2013. The Chemistry and Application of Dyes. Springer Science
509 and Business media.
510 Willets, J., Ashbolt, N., 2000. Understanding anaerobic decolorization of textile dye
511 wastewater: Mechanism and kinetics. Water Sci. Technol. 42, 409-415.
512 Xu, A., Brillas, E., Han, W., Wang, L., Sirés, I., 2019. On the positive effect of UVC light
513 during the removal of benzothiazoles by photoelectro-Fenton with UVA light. Appl.
514 Catal. B: Environ. 259, 118127.
515

Figure captions

Fig. 1. Influence of catalyst concentration on the change of (a) percentage of color removal, (b) normalized COD, (c) average current efficiency (in percentage), and (d) energy consumption per gram of COD with electrolysis time for the SPEF-like treatment of 6 L of 0.196 mM AR1 (4.06 mM of COD) solutions in 35 mM NaCl + 25 mM Na_2SO_4 at pH 3.0 using an FM01-LC reactor with a 64 cm^2 Ti|Ir–Sn–Sb oxide anode and a 64 cm^2 stainless steel cathode at current density (j) of 15 mA cm^{-2} and volumetric flow rate of 3.2 L min^{-1}. $[Fe^{2+}]_0$: (○) 0 mM (i.e., AO-HClO), (▲) 0.10 mM, (◆) 0.20 mM, (■) 0.30 mM, (▼) 0.40 mM and (●) 0.50 mM.

Fig. 2. Effect of current density on the time course of (a) percentage of color removal, (b) normalized COD, (c) average current efficiency (in percentage), and (d) energy consumption per gram of COD for the SPEF-like treatment of 6 L of 0.196 mM AR1 solutions in 35 mM NaCl + 25 mM Na_2SO_4 with 0.40 mM Fe^{2+} at pH 3.0 using an FM01-LC reactor with a Ti|Ir–Sn–Sb oxide anode and a stainless steel cathode at volumetric flow rate of 3.2 L min^{-1}. Applied j: (■) 5 mA cm^{-2}, (◆) 10 mA cm^{-2}, (▼) 15 mA cm^{-2} and (●) 20 mA cm^{-2}.

Fig. 3. Influence of initial AR1 dye concentration on the variation of (a) percentage of color removal, (b) normalized COD, (c) average current efficiency (in percentage), and (d) energy consumption per gram of COD with electrolysis time for the SPEF-like treatment of 6 L of AR1 solutions in 35 mM NaCl + 25 mM Na_2SO_4 with 0.4 mM Fe^{2+} at pH 3.0 using an FM01-LC reactor with a Ti|Ir–Sn–Sb oxide anode and a stainless steel cathode at j = 15 mA cm^{-2} and volumetric flow rate of 3.2 L min^{-1}. $[AR1]_0$: (●) 0.096 mM, (▼) 0.196 mM and (■) 0.385 mM.

538 **Fig. 4**. Variation of (a) percentage of color removal, (b) normalized COD, (c) average current
539 efficiency (in percentage), and (d) energy consumption per gram of COD with electrolysis
540 time for the (○) AO-HClO, (▲) EF-like, (◆) PEF-like and (▼) SPEF-like treatment of 6 L
541 of 0.196 mM AR1 solutions in 35 mM NaCl + 25 mM Na_2SO_4 at pH 3.0 using an FM01-LC
542 reactor with a Ti|Ir–Sn–Sb oxide anode and a stainless steel cathode at j = 15 mA cm^{-2} and
543 volumetric flow rate of 3.2 L min^{-1}. The three latter methods were operated with 0.40 mM
544 Fe^{2+} as catalyst.

545 **Fig. 5**. Evolution of the concentration of (△,▲) maleic and (○,●) oxalic acids during the
546 (△,○) AO-HClO and (▲,●) EF-like treatments of Fig. 4.

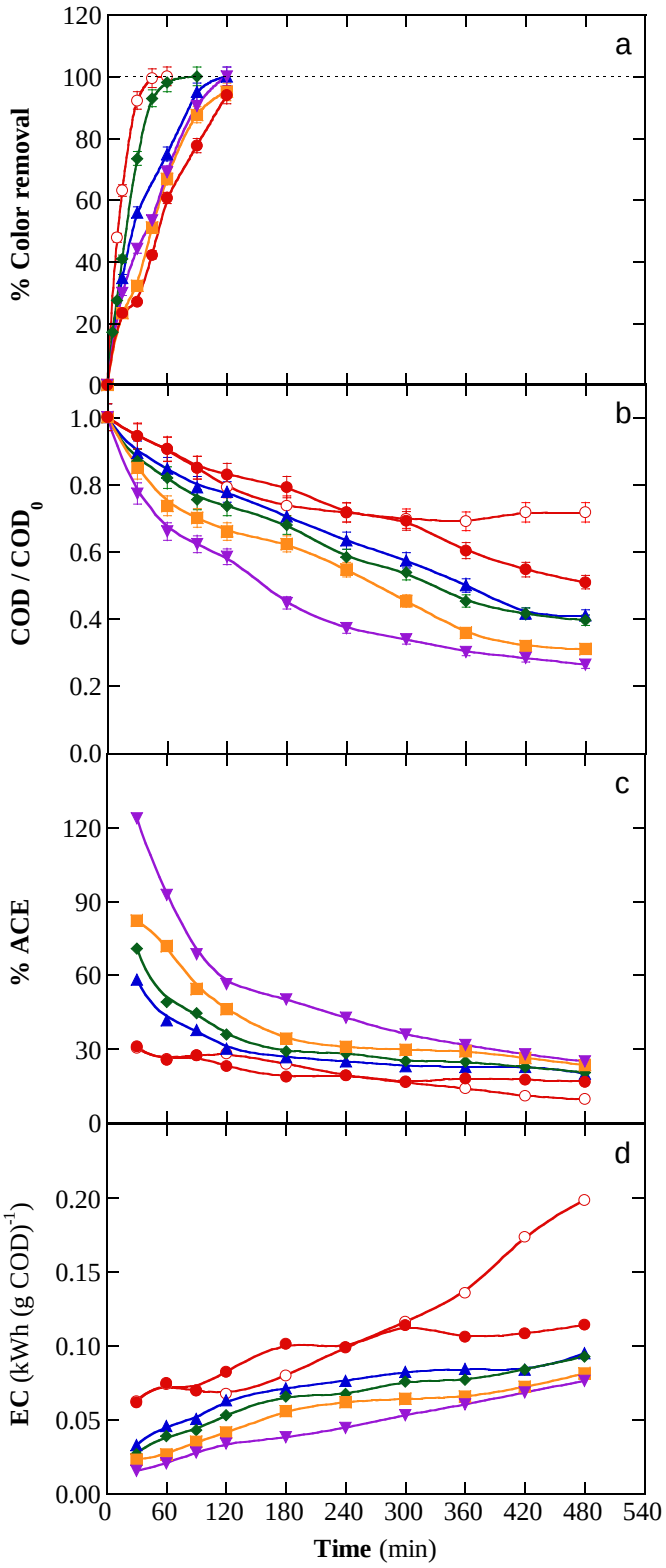
a
b
c
d
% Color removal
COD / COD0
% ACE
EC (kWh (g COD)-1)
Time (min)
0
20
40
60
80
100
120
0.0
0.2
0.4
0.6
0.8
1.0
30
90
0.00
0.05
0.10
0.15
0.20
0
60
120
180
240
300
360
420
480
540

Fig. 1

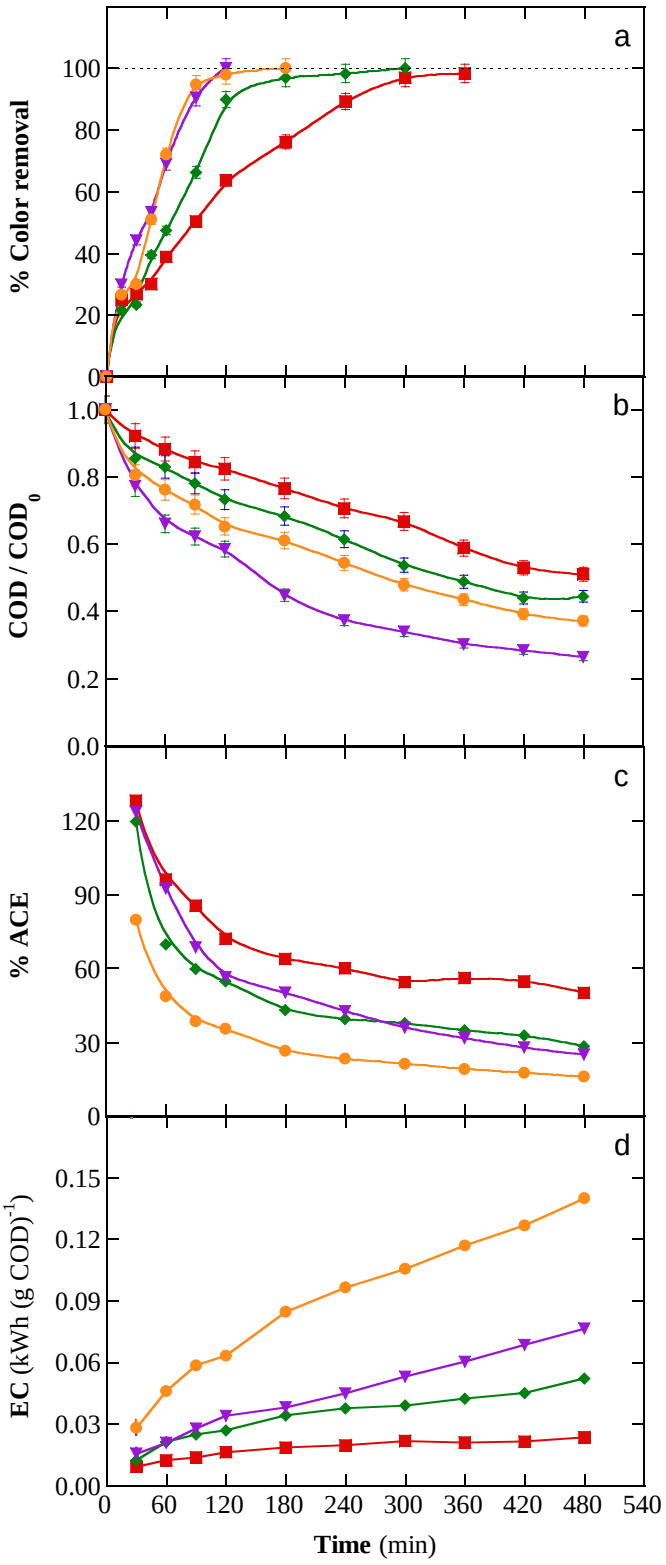
a
% Color removal
100
80
60
40
20
0
b
COD / COD0
1.0
0.8
0.6
0.4
0.2
0.0
c
% ACE
120
90
60
30
0
d
EC (kWh (g COD)-1)
0.15
0.12
0.09
0.06
0.03
0.00
0
60
120
180
240
300
360
420
480
540
Time (min)

Fig. 2

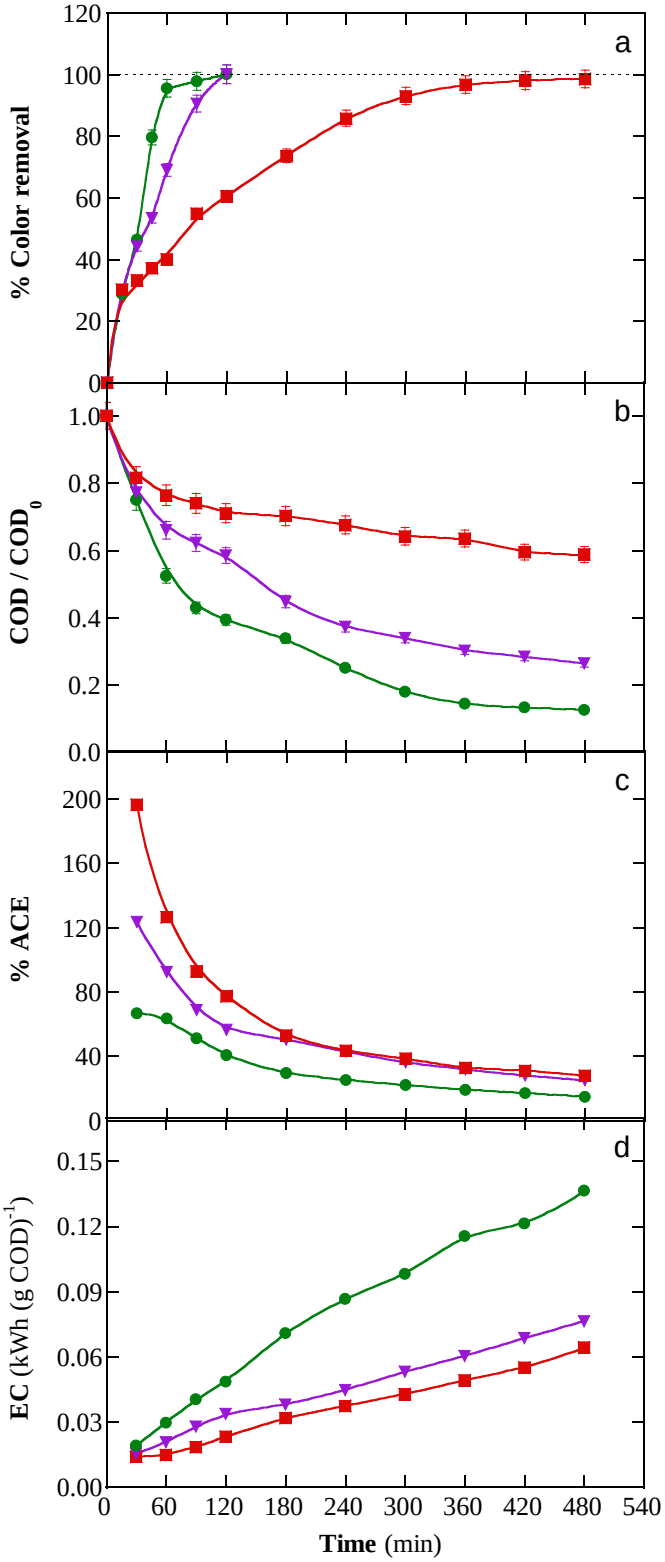
a
b
c
d
% Color removal
COD / COD0
% ACE
EC (kWh (g COD)-1)
Time (min)
0
20
40
60
80
100
120
0.0
0.2
0.4
0.6
0.8
1.0
40
80
120
160
200
0.00
0.03
0.06
0.09
0.12
0.15
0
60
120
180
240
300
360
420
480
540

Fig. 3

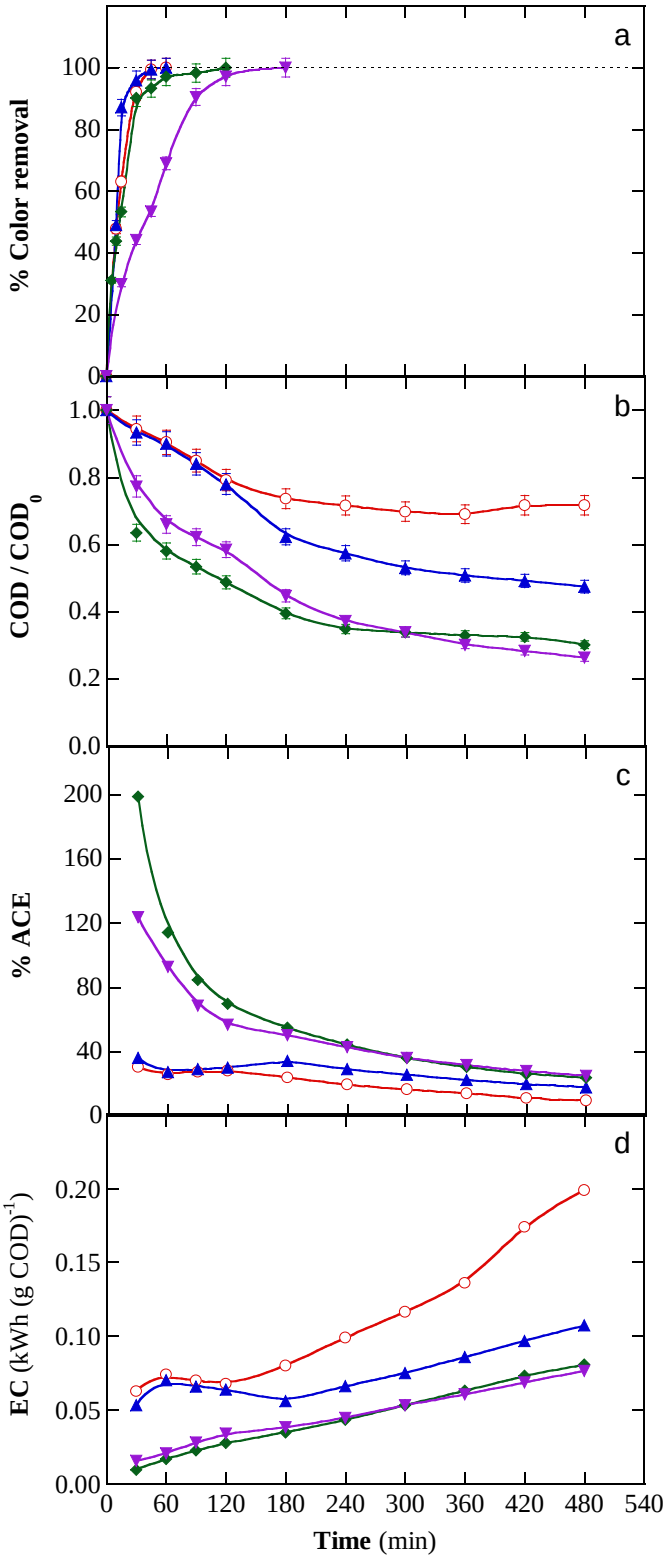
a
% Color removal
100
80
60
40
20
0
b
COD / COD0
1.0
0.8
0.6
0.4
0.2
0.0
c
% ACE
200
160
120
80
40
0
d
EC (kWh (g COD)-1)
0.20
0.15
0.10
0.05
0.00
0
60
120
180
240
300
360
420
480
540
Time (min)

Fig. 4

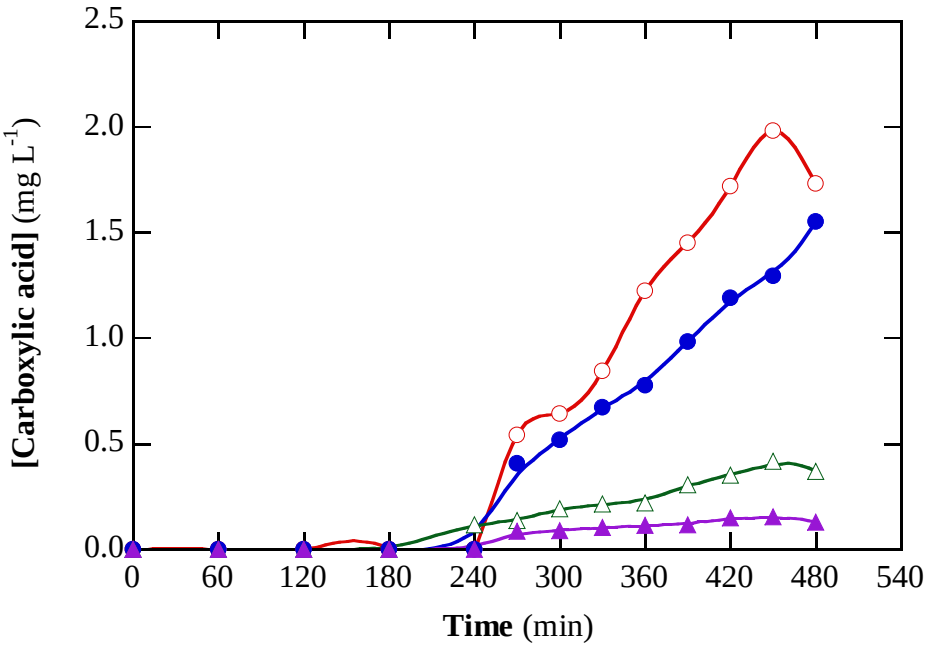
2.5
2.0
1.5
1.0
0.5
0.0
[Carboxylic acid] (mg L-1)
0
60
120
180
240
300
360
420
480
540
Time (min)

Fig. 5